Determination of the spacing between hydrogen-intercalated quasifreestanding monolayer graphene and 6*H*-SiC(0001) using total-reflection high-energy positron diffraction

Matthias Dodenhöft,[1] Izumi Mochizuki,[2] Ken Wada,[2] Toshio Hyodo,[2] Peter Richter,[3,4] Philip Schädlich,[3,4] Thomas Seyller,[3,4] and Christoph Hugenschmidt[1,*]

[1]*Forschungs-Neutronenquelle Heinz Maier-Leibnitz FRM II, Technische Universität München, Lichtenbergstraße 1, 85748 Garching, Germany*

[2]*Institute of Materials Structure Science, High Energy Accelerator Research Organization (KEK), Ibaraki 305-0801, Japan*

[3]*Institute for Physics, Technische Universität Chemnitz, Reichenhainer Straße 70, 09126 Chemnitz, Germany*

[4]*Center for Materials, Architectures and Integration of Nanomembranes (MAIN), Rosenbergstraße 6, 09126 Chemnitz, Germany*

(Received 27 June 2023; revised 2 September 2023; accepted 8 September 2023; published 31 October 2023)

We have investigated the structure of hydrogen-intercalated quasifreestanding monolayer graphene (QFMLG) grown on 6*H*-SiC(0001) by employing total-reflection high-energy positron diffraction. At least nine diffraction spots of the zeroth-order Laue zone were resolved along $\langle 11\bar{2}0\rangle$ and three along $\langle 1\bar{1}00\rangle$, which are assigned to graphene, SiC, and higher-order spots from multiple diffraction on both lattices. We further performed a rocking curve analysis based on the full dynamical diffraction theory to precisely determine the spacing between QFMLG and the SiC substrate. Our study yields a spacing of $d_{\mathrm{QFMLG}} = 4.18(6)$ Å that is in excellent agreement with the results from density-functional theory calculations published previously.

DOI: 10.1103/PhysRevB.108.155438

I. INTRODUCTION

Graphene has been extensively studied due to its exceptional properties, such as extremely high thermal conductivity [1] and mechanical strength [2,3], as well as massless charge carriers with unconventional behavior in tunneling, confinement, or magnetotransport [4–6]. Among different approaches to produce large-area graphene on an industrial scale, its synthesis on the surface of the wide band gap semiconductor SiC [7–9] is particularly appealing for high-power or high-frequency electronics. This is based on the fact that epitaxial graphene can be directly grown on SiC(0001) (without transfer), which is an intrinsic technological advantage.

Upon thermal decomposition, SiC(0001) exhibits a characteristic $(6\sqrt{3} \times 6\sqrt{3})R30^\circ$ surface reconstruction, which can be regarded as a precursor to the growth of graphene layers [10–12]. The associated buffer layer consists of carbon atoms and is covalently bound to the SiC substrate. Therefore, it has a corrugated structure [13,14] and is electrically inactive [15]. On the other hand, this interface also deteriorates the electronic properties of the adjacent graphene layer, leading to an intrinsic *n* doping, a long-range corrugation in the density of states, and a reduced, temperature-dependent charge carrier mobility [16–18].

Effective decoupling from the SiC substrate can be achieved by hydrogen intercalation, as first demonstrated by Riedl *et al.* [15]. At temperatures of $\sim 500\,^\circ$C, hydrogen can migrate below the buffer layer and break the covalent bonds with the substrate. The buffer layer is converted into quasifreestanding monolayer graphene (QFMLG), which resides on the H-terminated SiC(0001) surface [19,20]. Although there are other possibilities of interface manipulation, such as rapid cooling [21] or the intercalation of various other elements [22–26], hydrogen intercalation is considered to be the best approach for obtaining high-quality graphene [27].

In this study, we investigated the surface structure of hydrogen-intercalated QFMLG on 6*H*-SiC(0001) using total-reflection high-energy positron diffraction (TRHEPD) [28–31], i.e., positron diffraction in grazing incidence. In contrast to electrons, positrons experience a repulsive crystal potential that leads to an outstanding surface sensitivity. As demonstrated by Fukaya *et al.*, TRHEPD is particularly well suited to analyze the potential buckling of two-dimensional (2D) materials [32,33] and precisely determine the spacing between graphene and different substrates [34]. In an early study, Kawasuso *et al.* already investigated the surface graphitization and structure of few-layer graphene on 6*H*-SiC(0001) [35]. However, since then the theoretical understanding of the material system and the sample preparation has improved significantly, as well as the positron beam quality available for TRHEPD. Recently, Endo *et al.* investigated pristine and Ca-intercalated bilayer graphene grown on 6*H*-SiC(0001) [36].

II. EXPERIMENTAL PROCEDURE

As a prerequisite, TRHEPD requires a bright and coherent positron beam of adequate intensity. The measurements were therefore carried out at the Slow Positron Facility (SPF) of the Institute of Materials Structure Science, KEK in Japan [37,38]. Currently, this is the only operational TRHEPD setup in the world, although a second setup at the NEutron induced POsitron source MUniCh (NEPOMUC) [39,40] has

*christoph.hugenschmidt@frm2.tum.de

been developed recently [41]. A comprehensive overview of the measurement technique TRHEPD can be found elsewhere [30,31].

The QFMLG sample was prepared by polymer-assisted sublimation growth (PASG) of a buffer layer on 6*H*-SiC(0001) and subsequent hydrogen intercalation [9]. Prior to TRHEPD, the sample was comprehensively precharacterized using x-ray photoelectron spectroscopy (XPS), atomic force microscopy (AFM), and low-energy electron diffraction (LEED). This confirmed the presence of QFMLG and allows to exclude contaminations. Further details on the preparation parameters and the precharacterization can be found in the Supplemental Material S1 and S2, respectively [42–44].

After transfer to the TRHEPD ultrahigh vacuum (UHV) chamber at the SPF, the QFMLG sample was annealed *in situ* at 500 °C to remove surface adsorbates. To ensure a clean surface, we explicitly compared the effect of different annealing temperatures and durations on the basis of the obtained TRHEPD rocking curves [42,45,46]. All TRHEPD measurements were conducted at room temperature and we employed reflection high-energy electron diffraction (RHEED) for qualitative comparison. The incident, brightness-enhanced positron beam was set to an energy of 10 keV. Diffraction patterns were recorded along the azimuthal directions $\langle 11\bar{2}0\rangle$ and $\langle 1\bar{1}00\rangle$ (many-beam condition), as well as 7.5° off the high-symmetry directions (one-beam condition). In order to obtain the experimental rocking curves, i.e., the intensity of the specular spot as a function of the glancing angle θ, the sample was tilted in steps of 0.1° with respect to the incident positron beam. The intensity of the specular spot was extracted from the TRHEPD patterns following a standard routine [42].

III. RESULTS AND DISCUSSION

First, the positron diffraction patterns are discussed qualitatively by assignment of the observed diffraction spots. Subsequently, we employ a TRHEPD rocking curve analysis to determine the interlayer spacing between QFMLG and the SiC substrate.

A. Positron diffraction patterns

Two TRHEPD patterns for $\theta = 5.5°$ are shown in Figs. 1(a) and 1(b). We observe at least nine diffraction spots along $\langle 11\bar{2}0\rangle$ and three along $\langle 1\bar{1}00\rangle$. Additionally, we can identify very faint Kikuchi lines, which are much less pronounced than in RHEED. This is related to the shallower probing depth of TRHEPD due to the repulsive crystal potential for positrons [47].

Following the LEED analysis [42], we expect the TRHEPD patterns to be composed of diffraction spots from graphene and SiC, which are superimposed by further spots that stem from multiple diffraction on both lattices. Since the lattices of graphene and SiC are rotated by 30° with respect to each other, the main diffraction spots are observed along different crystallographic directions. Due to the different lattice constants, the spacing of the graphene spots on the Laue semicircle must be greater than for SiC [48]. Therefore, we can assign the two bright spots in Fig. 1(a) to graphene and those in Fig. 1(b) to SiC. The ratio of the respective horizontal spacings is approximately 1.29, which agrees reasonably well with the calculated inverse ratio of the lattice constants of ∼1.25. Interestingly, we find that the intensity of the graphene spots is much larger than those of SiC, although only the topmost surface layer is composed of graphene. This is explained by the exceptional surface sensitivity of TRHEPD, even at such large glancing angle. For comparison, we refer to the LEED

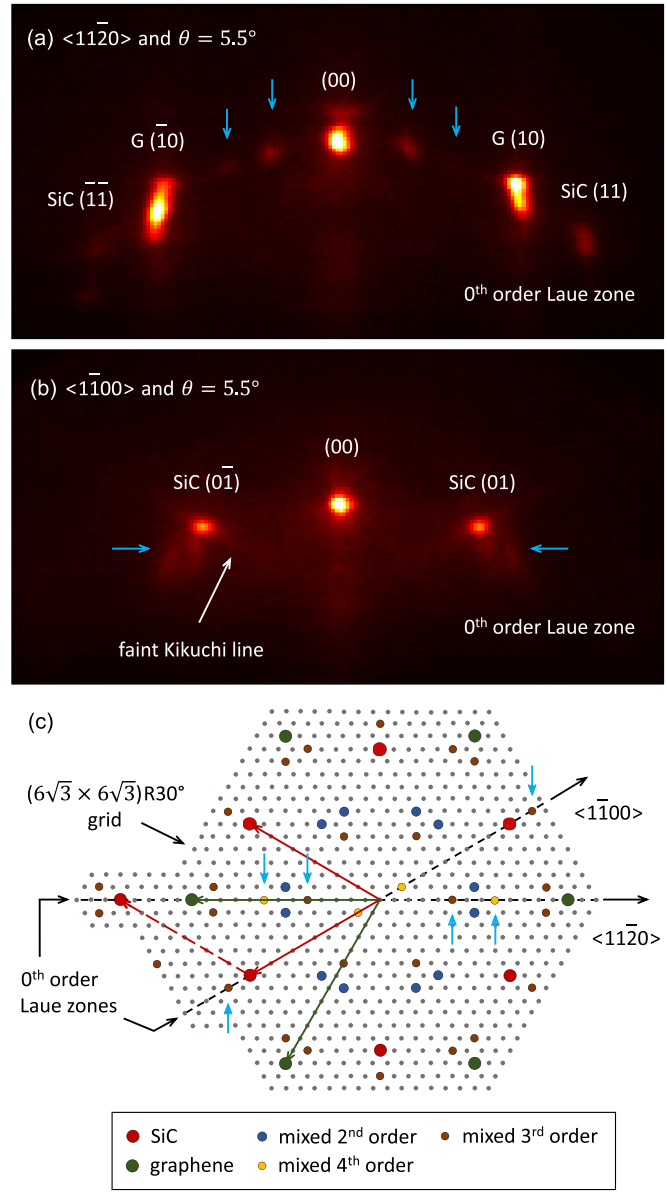

FIG. 1. TRHEPD patterns of QFMLG along high-symmetry directions (integration time 40 min, linear color scale). (a) The bright diffraction spots along $\langle 11\bar{2}0\rangle$ are assigned to the graphene lattice. Only the zeroth-order Laue zone is resolved. (b) The two pronounced spots along $\langle 1\bar{1}00\rangle$ are assigned to the SiC lattice. Faint Kikuchi lines can be observed as well. (c) Reciprocal space: $(6\sqrt{3} \times 6\sqrt{3})R30°$ grid with SiC (red) and graphene (green) lattice vectors and points. Higher-order spots that stem from multiple diffraction on both lattices are marked as well (not all fourth-order spots are shown). The blue arrows indicate the mixed higher-order spots that are assigned in (a) and (b), respectively.

pattern shown in Fig. S3(a) of the Supplemental Material [42], where the SiC spots are more pronounced indicating a deeper mean probing depth.

For the assignment of the remaining diffraction spots, we refer to Fig. 1(c), which is a map of reciprocal space including (mixed) higher-order diffraction spots. The blue arrows indicate the relevant mixed order spots that coincide with the zeroth-order Laue zones. For the measurement along $\langle 11\bar{2}0\rangle$, all four spots are clearly resolved and the relative intensities of third and fourth order support this assignment. With respect to the SiC lattice, these spots are located at $\pm(5/18, 5/18)$ and $\pm(8/18, 8/18)$, respectively. The two minor diffraction spots further outside on the Laue semicircle in Fig. 1(a) can be assigned to the (11) and $(\bar{1}\bar{1})$ reflections of SiC. For the measurement along $\langle 1\bar{1}00\rangle$, we expect to see the two mixed third-order spots close to the SiC (01) and $(0\bar{1})$ reflections. However, these spots are kind of smeared out in the diffraction pattern and it is challenging to determine their exact location.

B. Rocking curve analysis

The intensities of the TRHEPD rocking curves were calculated numerically based on the full dynamical diffraction theory [49–51]. To account for the finite size of the sample, the calculated intensities were scaled by the geometrical factor $\sin\theta$. The average crystal potential was set to 11.5 eV for graphene [34], whereas the value for SiC was fine tuned to 17.1 eV to match the experimentally observed Bragg peaks [52]. We employed the Nelder-Mead algorithm to minimize the difference between the calculated and experimental rocking curves by adjusting the parameters of the established structure model [53]. The agreement of the fit was quantified using the reliability factor [30]

$$R = \sqrt{\sum_i [I_{\mathrm{expt}}(\theta_i) - I_{\mathrm{calc}}(\theta_i)]^2}, \qquad (1)$$

where $I_{\mathrm{expt}}(\theta_i)$ and $I_{\mathrm{calc}}(\theta_i)$ are the normalized experimental and calculated intensities of the specular spot at the glancing angles θ_i.

The open symbols in Fig. 2(a) represent the experimental rocking curve obtained under the one-beam condition where the contribution of in-plane diffraction is strongly suppressed [54]. The one-beam analysis thus allows the determination of the out-of-plane atomic coordinates and yields the separation of atomic layers when including their mean composition and occupation [55]. The calculations were first carried out for a simple model assuming a fully occupied graphene layer without surface roughness or bilayer fraction. However, this model failed to reproduce the shoulder observed in the region of total reflection at 1.6°. At the same position, Kawasuso *et al.* observed a pronounced dip structure, which was essentially attributed to atomic-scale surface roughness [28,52,56]. We found that the shoulder can be well reproduced by including a small fraction of bilayer graphene. The best fit is the solid red line shown in Fig. 2(a), which yields a reliability factor of 1.1%. The precisely known bulk lattice parameters of SiC were fixed, but we considered the possible relaxation of the uppermost Si layer. Since the flat structure of QFMLG has already been confirmed by other

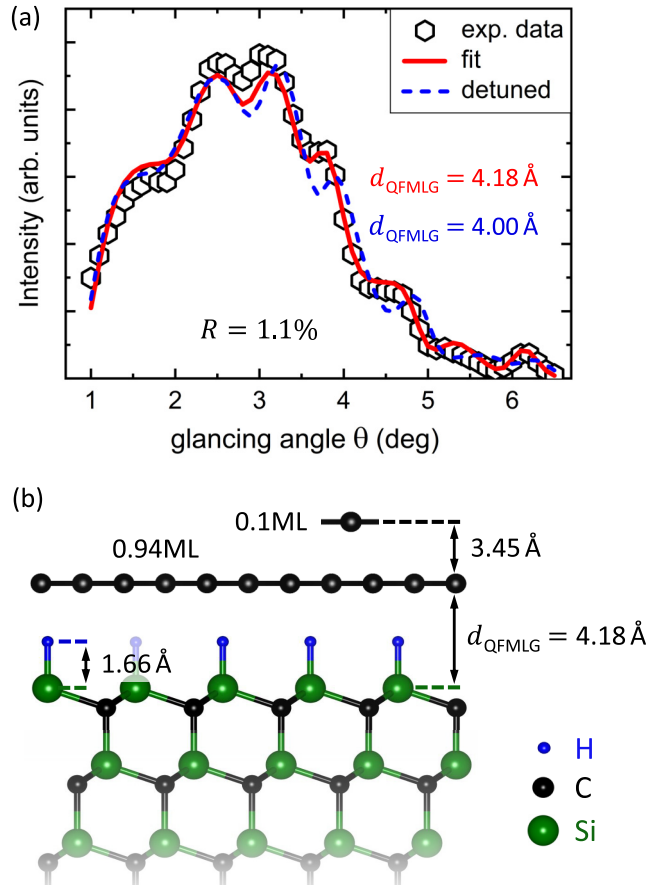

FIG. 2. TRHEPD one-beam rocking curve analysis of QFMLG. The calculation is based on the structure depicted in (b), including six fit parameters, i.e., occupations and spacings of QFMLG and graphene bilayer, the spacing of the hydrogen atoms, and the lattice relaxation of the top Si layer. The structural parameters were extracted from the fit in (a) (red line). The rocking curve is particularly sensitive to the spacing d_{QFMLG}: When detuned by 0.18 Å (dashed blue line), the R factor increases from 1.1% to 1.7% and some features change completely.

studies [53], we neglected buckling in the final fit to prevent overfitting. The results from the fit are listed in Table I and the associated structure is schematically depicted in Fig. 2(b).

We emphasize that the rocking curve is particularly sensitive to the parameter d_{QFMLG}, i.e., the spacing between QFMLG and the SiC substrate. This can be illustrated by deliberately detuning d_{QFMLG}, as shown by the dashed blue line in Fig. 2(a). When the optimum value is reduced by only 0.18 Å, several features change completely, e.g., the shoulder at $\sim 4.6°$ becomes a minimum and the reliability factor increases to 1.7% (or at best to 1.5% by readjusting all other parameters). Conversely, the strong influence on the rocking curve allows us to determine d_{QFMLG} with the highest precision. In fact, already the first structure model (without bilayer occupation) yields very consistent results. In contrast, the uncertainties of the other parameters are significantly higher. The TRHEPD signal generally tends to be more sensitive to heavier atoms due to their increased atomic scattering factors [57]. In agreement with this, we observe that

TABLE I. Structural parameters of QFMLG extracted from the fit shown in Fig. 2(a). The spacings d_{BL}, d_{QFMLG}, and d_H are defined with respect to the position of the top Si layer (relaxed by Δz_{Si}).

Bilayer fraction		QFMLG		Hydrogen	Top Si layer
Occupation	d_{BL} (Å)	Occupation	d_{QFMLG} (Å)	d_H (Å)	Δz_{Si} (Å)
9.8%	7.63 ± 0.20	93.9%	4.18 ± 0.06	1.66 ± 0.25	-0.01 ± 0.05

the variation of the spacing of the hydrogen layer has very little effect on the rocking curve. Consequently, the uncertainty is relatively high and other techniques, such as infrared spectroscopy, are better suited to precisely determine the Si-H bond length. Furthermore, we point out that the calculation did not explicitly consider bilayer domains, but individual C atoms that are distributed on the surface. In combination with the reduced occupation of the QFMLG layer, this can be interpreted as surface roughness that might originate from the sample preparation or intrinsic defects. The best fit yields a bilayer spacing of 3.45 Å with respect to the QFMLG layer, which is slightly larger than the interlayer spacing in graphite [58].

The rocking curves obtained under the many-beam condition along $\langle 11\bar{2}0\rangle$ and $\langle 1\bar{1}00\rangle$ are shown in Figs. 3(a) and 3(b), respectively. Since the exact in-plane coordinates of pristine graphene are known and the interaction with the SiC substrate

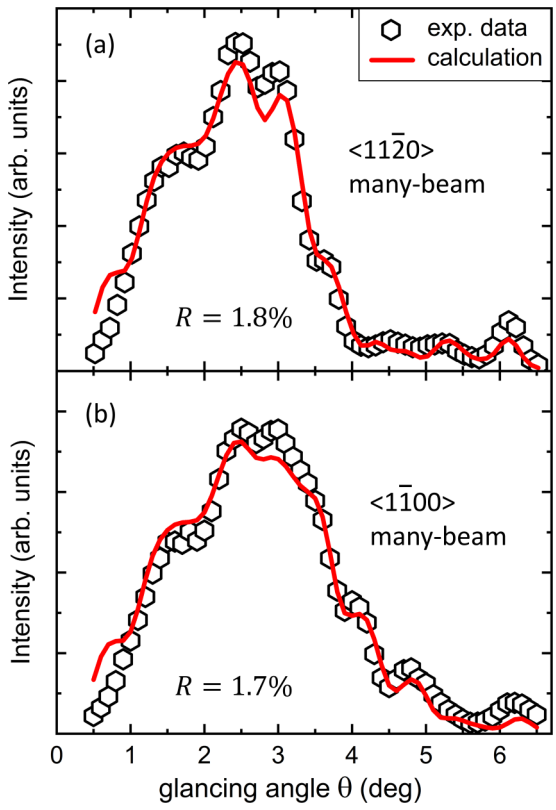

FIG. 3. TRHEPD many-beam rocking curve analysis of QFMLG along (a) $\langle 11\bar{2}0\rangle$ and (b) $\langle 1\bar{1}00\rangle$. The calculations were done for the structural parameters obtained from the one-beam analysis (see Table I) and the literature values for the in-plane coordinates of graphene and SiC.

is relatively weak, the many-beam data were mainly used for a sanity check of the obtained results. The calculations were thus performed for fixed parameters, i.e., without employing the Nelder-Mead algorithm. For both directions we obtain good agreement with reliability factors of 1.8% and 1.7%, respectively. We observe that the calculated curves deviate from the experimental data for very small glancing angles below 1° due to the significant decrease in intensity for geometrical reasons. We find that the shoulder at ∼1.6° is well reproduced by the bilayer occupation determined before. Interestingly, the agreement in the angular range above 4° is noticeably worse than for the one-beam data. This is most likely related to the presence of different stacking terminations of 6*H*-SiC(0001), as associated with terrace steps of different heights [59,60]. Since step bunching is not dominant for PASG, the signal from different stacking terminations with distinct in-plane structures is superimposed. For the one-beam analysis, this has essentially no effect because the vertical spacings are the same for all stacking orders. However, it affects the many-beam rocking curve, particularly with increasing probing depth, i.e., for large glancing angles. In the calculations, on the other hand, we only considered one specific stacking termination due to computational constraints. Regardless of this, altogether the many-beam data support the findings from the one-beam analysis, e.g., the presence of a small fraction of bilayer graphene associated with surface roughness and the found interlayer spacing d_{QFMLG}.

Sforzini *et al.* performed density-functional theory (DFT) calculations of the full supercell of QFMLG on 6*H*-SiC(0001) within the generalized gradient approximation (GGA) and by employing the Perdew-Burke-Ernzerhof (PBE) functional with a correction for van der Waals effects [53]. Our experimental result of $d_{QFMLG,TRHEPD} = (4.18 \pm 0.06)$ Å is in excellent agreement with the calculated value of $d_{QFMLG,DFT} = 4.16$ Å, highlighting the strength of TRHEPD rocking curve analysis. In contrast, other studies based on normal incidence x-ray standing wave (NIXSW) [53] or high-resolution x-ray reflectivity (XRR) measurements [61] yield a marginally larger spacing of $d_{QFMLG,NIXSW} = (4.22 \pm 0.06)$ Å which coincides with theory just within the uncertainty range. Moreover, we note that the obtained surface relaxations of the substrate layers are particularly large in the NIXSW study, which is inconsistent.

IV. CONCLUSION

We performed TRHEPD measurements to investigate the surface structure of hydrogen-intercalated QFMLG epitaxially grown on 6*H*-SiC(0001). The observed diffraction spots were assigned to graphene, SiC, and higher-order spots that stem from multiple diffraction on both lattices. In contrast to

LEED and RHEED, the graphene spots in the TRHEPD patterns were found to be much brighter than those of SiC due to the outstanding surface sensitivity of positron diffraction. For the quantitative analysis, we compared the experimental rocking curves with those calculated from the established structure model. Under the one-beam condition, the rocking curve of QFMLG was found to be particularly sensitive to the spacing between the graphene layer and SiC substrate. Compared to previous experimental studies based on NIXSW or XRR, we find a slightly smaller spacing of $d_{\mathrm{QFMLG}} = (4.18 \pm 0.06)$ Å, which is in excellent agreement with the value predicted by DFT calculations.

ACKNOWLEDGMENTS

We thank Florian Speck for his support and discussions. Financial support by the German federal ministry of education and research (BMBF) within Project No. 05K16WO7 is gratefully acknowledged.

[1] A. A. Balandin, S. Ghosh, W. Bao, I. Calizo, D. Teweldebrhan, F. Miao, and C. N. Lau, Nano Lett. **8**, 902 (2008).
[2] C. Lee, X. Wei, J. W. Kysar, and J. Hone, Science **321**, 385 (2008).
[3] K. Cao, S. Feng, Y. Han, L. Gao, T. H. Ly, Z. Xu, and Y. Lu, Nat. Commun. **11**, 284 (2020).
[4] K. S. Novoselov, A. K. Geim, S. V. Morozov, D. Jiang, M. I. Katsnelson, I. V. Grigorieva, S. V. Dubonos, and A. A. Firsov, Nature (London) **438**, 197 (2005).
[5] M. Katsnelson, K. Novoselov, and A. Geim, Nat. Phys. **2**, 620 (2006).
[6] A. H. Castro Neto, F. Guinea, N. M. R. Peres, K. S. Novoselov, and A. K. Geim, Rev. Mod. Phys. **81**, 109 (2009).
[7] W. A. de Heer, C. Berger, X. Wu, P. N. First, E. H. Conrad, X. Li, T. Li, M. Sprinkle, J. Hass, M. L. Sadowski, M. Potemski, and G. Martinez, Solid State Commun. **143**, 92 (2007).
[8] K. Emtsev, A. Bostwick, K. Horn, J. Jobst, G. L. Kellogg, L. Ley, J. L. McChesney, T. Ohta, S. A. Reshanov, J. Röhrl, E. Rotenberg, A. K. Schmid, D. Waldmann, H. B. Weber, and T. Seyller, Nat. Mater. **8**, 203 (2009).
[9] M. Kruskopf, D. M. Pakdehi, K. Pierz, S. Wundrack, R. Stosch, T. Dziomba, M. Götz, J. Baringhaus, J. Aprojanz, C. Tegenkamp, J. Lidzba, T. Seyller, F. Hohls, F. J. Ahlers, and H. W. Schumacher, 2D Mater. **3**, 041002 (2016).
[10] A. J. V. Bommel, J. E. Crombeen, and A. V. Tooren, Surf. Sci. **48**, 463 (1975).
[11] I. Forbeaux, J.-M. Themlin, and J.-M. Debever, Phys. Rev. B **58**, 16396 (1998).
[12] U. Starke and C. Riedl, J. Phys.: Condens. Matter **21**, 134016 (2009).
[13] F. Varchon, P. Mallet, J.-Y. Veuillen, and L. Magaud, Phys. Rev. B **77**, 235412 (2008).
[14] S. Goler, C. Coletti, V. Piazza, P. Pingue, F. Colangelo, V. Pellegrini, K. V. Emtsev, S. Forti, U. Starke, F. Beltram, and S. Heun, Carbon **51**, 249 (2013).
[15] C. Riedl, C. Coletti, T. Iwasaki, A. A. Zakharov, and U. Starke, Phys. Rev. Lett. **103**, 246804 (2009).
[16] T. Ohta, A. Bostwick, J. L. McChesney, T. Seyller, K. Horn, and E. Rotenberg, Phys. Rev. Lett. **98**, 206802 (2007).
[17] C. Riedl, C. Coletti, and U. Starke, J. Phys. D: Appl. Phys. **43**, 374009 (2010).
[18] J. Jobst, D. Waldmann, F. Speck, R. Hirner, D. K. Maude, T. Seyller, and H. B. Weber, Phys. Rev. B **81**, 195434 (2010).
[19] F. Speck, J. Jobst, F. Fromm, M. Ostler, D. Waldmann, M. Hundhausen, H. B. Weber, and Th. Seyller, Appl. Phys. Lett. **99**, 122106 (2011).
[20] F. Speck, M. Ostler, S. Besendörfer, J. Krone, M. Wanke, and T. Seyller, Ann. Phys. **529**, 1700046 (2017).
[21] J. Bao, W. Norimatsu, H. Iwata, K. Matsuda, T. Ito, and M. Kusunoki, Phys. Rev. Lett. **117**, 205501 (2016).
[22] I. Gierz, T. Suzuki, R. T. Weitz, D. S. Lee, B. Krauss, C. Riedl, U. Starke, H. Höchst, J. H. Smet, C. R. Ast, and K. Kern, Phys. Rev. B **81**, 235408 (2010).
[23] A. L. Walter, K.-J. Jeon, A. Bostwick, F. Speck, M. Ostler, T. Seyller, L. Moreschini, Y. S. Kim, Y. J. Chang, K. Horn, and E. Rotenberg, Appl. Phys. Lett. **98**, 184102 (2011).
[24] S. Forti, A. Stöhr, A. A. Zakharov, C. Coletti, K. V. Emtsev, and U. Starke, 2D Mater. **3**, 035003 (2016).
[25] P. D. Bentley, T. W. Bird, A. P. J. Graham, O. Fossberg, S. P. Tear, and A. Pratt, AIP Adv. **11**, 025314 (2021).
[26] A. A. Rybkina, S. O. Filnov, A. V. Tarasov, D. V. Danilov, M. V. Likholetova, V. Y. Voroshnin, D. A. Pudikov, D. A. Glazkova, A. V. Eryzhenkov, I. A. Eliseyev, V. Y. Davydov, A. M. Shikin, and A. G. Rybkin, Phys. Rev. B **104**, 155423 (2021).
[27] R. Sakakibara and W. Norimatsu, Phys. Rev. B **105**, 235442 (2022).
[28] A. Ichimiya, Solid State Phenom. **28-29**, 143 (1992).
[29] A. Kawasuso and S. Okada, Phys. Rev. Lett. **81**, 2695 (1998).
[30] Y. Fukaya, A. Kawasuso, A. Ichimiya, and T. Hyodo, J. Phys. D: Appl. Phys. **52**, 013002 (2019).
[31] C. Hugenschmidt, Surf. Sci. Rep. **71**, 547 (2016).
[32] Y. Fukaya, I. Mochizuki, M. Maekawa, K. Wada, T. Hyodo, I. Matsuda, and A. Kawasuso, Phys. Rev. B **88**, 205413 (2013).
[33] Y. Fukaya, I. Matsuda, B. Feng, I. Mochizuki, T. Hyodo, and S. Shamoto, 2D Mater. **3**, 035019 (2016).
[34] Y. Fukaya, S. Entani, S. Sakai, I. Mochizuki, K. Wada, T. Hyodo, and S. Shamoto, Carbon **103**, 1 (2016).
[35] A. Kawasuso, M. Maekawa, M. Yoshikawa, and A. Ichimiya, Appl. Surf. Sci. **244**, 149 (2005).
[36] Y. Endo, Y. Fukaya, I. Mochizuki, A. Takayama, T. Hyodo, and S. Hasegawa, Carbon **157**, 857 (2020).
[37] K. Wada, T. Hyodo, A. Yagishita, M. Ikeda, S. Ohsawa, T. Shidara, K. Michishio, T. Tachibana, Y. Nagashima, Y. Fukaya, M. Maekawa, and A. Kawasuso, Eur. Phys. J. D **66**, 37 (2012).
[38] M. Maekawa, K. Wada, Y. Fukaya, A. Kawasuso, I. Mochizuki, T. Shidara, and T. Hyodo, Eur. Phys. J. D **68**, 165 (2014).
[39] C. Hugenschmidt, C. Piochacz, M. Reiner, and K. Schreckenbach, New J. Phys. **14**, 055027 (2012).
[40] C. Hugenschmidt, H. Ceeh, T. Gigl, F. Lippert, C. Piochacz, M. Reiner, K. Schreckenbach, S. Vohburger, J. Weber, and S. Zimnik, J. Phys.: Conf. Ser. **505**, 012029 (2014).
[41] M. Dodenhöft, S. Vohburger, and C. Hugenschmidt, Rev. Sci. Instrum. **92**, 115103 (2021).

[42] See Supplemental Material at http://link.aps.org/supplemental/10.1103/PhysRevB.108.155438 for additional information on the sample preparation as well as precharacterization by x-ray photoelectron spectroscopy (XPS), atomic force microscopy (AFM), and low-energy electron diffraction (LEED), as well as an outline of TRHEPD data processing, which includes Refs. [43–46].

[43] NIST X-ray Photoelectron Spectroscopy Database, doi:10.18434/T4T88K (2000).

[44] K. V. Emtsev, F. Speck, T. Seyller, L. Ley, and J. D. Riley, Phys. Rev. B **77**, 155303 (2008).

[45] C. Virojanadara, A. A. Zakharov, R. Yakimova, and L. I. Johansson, Surf. Sci. **604**, L4 (2010).

[46] N. Sieber, T. Seyller, L. Ley, D. James, J. D. Riley, R. C. G. Leckey, and M. Polcik, Phys. Rev. B **67**, 205304 (2003).

[47] Y. Fukaya, M. Maekawa, A. Kawasuso, I. Mochizuki, K. Wada, T. Shidara, A. Ichimiya, and T. Hyodo, Appl. Phys. Express **7**, 056601 (2014).

[48] J. E. Boschker, L. A. Galves, T. Flissikowski, J. M. J. Lopes, H. Riechert, and R. Calarco, Sci. Rep. **5**, 18079 (2016).

[49] A. Ichimiya, Jpn. J. Appl. Phys. **22**, 176 (1983).

[50] T. Hanada, H. Daimon, and S. Ino, Phys. Rev. B **51**, 13320 (1995).

[51] K. Tanaka, T. Hoshi, I. Mochizuki, T. Hanada, A. Ichimiya, and T. Hyodo, Acta Phys. Pol. A **137**, 188 (2020).

[52] A. Kawasuso, T. Ishimoto, Y. Fukaya, K. Hayashi, and A. Ichimiya, e-J. Surf. Sci. Nanotechnol. **1**, 152 (2003).

[53] J. Sforzini, L. Nemec, T. Denig, B. Stadtmüller, T. L. Lee, C. Kumpf, S. Soubatch, U. Starke, P. Rinke, V. Blum, F. C. Bocquet, and F. S. Tautz, Phys. Rev. Lett. **114**, 106804 (2015).

[54] A. Ichimiya, Surf. Sci. **192**, L893 (1987).

[55] A. Ichimiya and P. I. Cohen, *Reflection High Energy Electron Diffraction* (Cambridge University Press, Cambridge, UK, 2004).

[56] A. Kawasuso, K. Kojima, M. Yoshikawa, H. Itoh, and K. Narumi, Appl. Phys. Lett. **76**, 1119 (2000).

[57] T. Hoshi, D. Sakata, S. Oie, I. Mochizuki, S. Tanaka, T. Hyodo, and K. Hukushima, Comput. Phys. Commun. **271**, 108186 (2022).

[58] Y. Baskin and L. Meyer, Phys. Rev. **100**, 544 (1955).

[59] *Silicon Carbide Recent Major Advances*, edited by W. J. Choyke, H. Matsunami, and G. Pensl (Springer, Berlin, 2004).

[60] D. M. Pakdehi, P. Schädlich, T. T. N. Nguyen, A. A. Zakharov, S. Wundrack, E. Najafidehaghani, F. Speck, K. Pierz, T. Seyller, C. Tegenkamp, and H. W. Schumacher, Adv. Funct. Mater. **30**, 2004695 (2020).

[61] J. D. Emery, V. D. Wheeler, J. E. Johns, M. E. McBriarty, B. Detlefs, M. C. Hersam, D. K. Gaskill, and M. J. Bedzyk, Appl. Phys. Lett. **105**, 161602 (2014).